THE CATHOLIC UNIVERSITY OF AMERICA
DEPARTMENT OF ELECTRICAL ENGINEERING

TESTING OF FTS FINGERS AND INTERFACE USING A PASSIVE COMPLIANT ROBOT MANIPULATOR

by

Charles C. Nguyen
Principal Investigator and Professor

and

Sami S. Antrazi
Graduate Research Assistant

submitted to
Mr. Lloyd Purves and Mr. John M. Vranish
Code 714
Goddard Space Flight Center (NASA)
Greenbelt, Maryland

April 1992

REPORT SUMMARY

This semiannual report presents the results obtained from the research grant "A Study of Space-Rated Connectors Using A Robot End-Effector," sponsored by the Goddard Space Flight Center (NASA), for the period between September 1, 1991 and February 29, 1992.

This report deals with testing of a pair of robot fingers designed for the Flight Telerobot Servicer (FTS) to grasp a cylinder type of Orbital Replaceable Unit (ORU) interface. The report first presents the objectives of the study and then describes the testbed consisting of a Stewart Platform-based manipulator equipped with a passive compliant platform which also serves as a force/torque sensor. Kinematic analysis is then performed to provide a closed-form solution for the force inverse kinematics and iterative solution for the force forward kinematics using the Newton's Raphson Method. Mathematical expressions are then derived to compute forces/torques applied to the FTS fingers during the mating/demating with the interface. After that, the report presents the results of the experimental study conducted to investigate the characteristics and feasibility of the fingers. The experimental study is composed of three parts. The first part is devoted to obtain data of forces applied by the finger to the interfaces under various translational and rotational misalignments, the second part to determine the maximum allowed capture angles to ensure successful mating, and the third part to process and interpret the obtained forces/torques data.

Contents

1 Introduction 1

2 Objectives of the Study 1

3 The Robotic Testbed 1
- 3.1 The 6 DOF Robot Manipulator 2
- 3.2 The Passive Compliant Force/Torque Sensor 2
- 3.3 The Force Data Acquisition System 3

4 The Inverse Kinematic Transformation 3

5 The Forward Kinematic Transformation 5

6 Computation of Forces/Torques 6

7 Test Procedures 7

8 Experimental Study Results 8
- 8.1 Capture Ranges 8
- 8.2 Graphical Representation of Test Results 8

9 Conclusions and Recommendations 11

1 Introduction

On-orbit maintenance of Orbit Replaceable Units (ORU) may be performed by astronauts during an Extra Vehicular Activity (EVA). The astronaut is required to possess the ability to effectively and safely adapt to space, an environment which is not precisely controllable and fully understood *a priori* as an earth-based factory environment. Recognizing the danger of space operations astronauts are exposed to, NASA has set the overall goal of the Space Station Freedom (SSF) program to minimize the number of required EVA's and to emphasize on developing robot-friendly hardwares and telerobots which will replace or assist astronauts in performing EVAs. Consequently on-orbit maintenance of Orbit Replaceable Units (ORU) will be primarily performed through the use of telerobots [1].

This report presents results obtained from the study of characteristics and feasibility of a pair of robot fingers designed to be used with the Flight Telerobot Servicer (FTS). The fingers are used to grasp an ORU interface of *cylinder type*. This report is organized as follows. First Section 2 lists the objectives of the study. The main components of the testbed which was employed in the study are presented in Section 3. Section 4 and 5 presents the development of the testbed force inverse kinematic and forward kinematic transformations, respectively. After that, in Section 6, mathematical expressions are derived to compute forces/torques applied to the FTS fingers. The test procedures are described in Section 7. Finally, Section 8 presents results of numerous experiments conducted to study the characteristics and feasibility of the fingers in mating/demating with the interface.

2 Objectives of the Study

The objectives of the study are presented as follows:

1. To study the operation and seating characteristics of the FTS fingers and the mating feasibility of the fingers with the cylinder interface using a robot gripper.

2. To measure capture angles, maximum allowed lateral and rotational misalignments of the FTS fingers.

3. To study the impact of forces/torques created by mating of the FTS finger with its interface under lateral and rotational misalignments.

4. To measure the forces, torques and passive compliance required for successful mating of the fingers with its interface without damaging the fingers and the interface.

3 The Robotic Testbed

In this section, we briefly describe the main components and operations of the testbed used in the study of the FTS fingers. The testbed is mainly composed of a 6 degree-of-freedom (DOF) robot manipulator, a force/torque sensor and a data acquisition system, which are described below.

3.1 The 6 DOF Robot Manipulator

Figures 1 shows the robot manipulator whose design was based on the mechanism of the Stewart Platform [2]. The manipulator mainly consists of a lower base platform, an upper payload platform, and six linear actuators. The movable payload platform is supported above the stationary base platform by the linear actuators consisting of ballnuts and ballscrews providing the extensibility. Stepper motors were selected to drive the ballscrews to extend or shorten the actuator lengths whose variations will in turn produce the motion of the payload platform. Each end of the actuator links is mounted to the platforms by 2 rotary joints whose axes intersect and are perpendicular to each other. The rotation of each stepper motor is controlled by sending out proper commands to an indexer which then transmits proper pulse sequences to the stepper motor drive. Therefore, precise gripper motion can be produced by properly controlling the motions of six manipulator legs. A Cartesian path specified with desired starting and ending velocities and accelerations is converted into 6 Cartesian trajectories using a Cartesian trajectory planning scheme. Then based upon the desired Cartesian trajectories, joint-space trajectories will be determined by a planner which sends proper commands through the RS232 port of a personal computer to the indexers. The indexer will then transmit pulses to the stepper motor drives where microstepping permits each revolution (360^0) of the stepper motor to be equivalent to 25,000 steps. Therefore the drive rotates the stepper motor one angular increment of $\frac{360^0}{25{,}000} = 0.0144^o$, each time it receives one step pulse. Furthermore, through the linear motion converter system consisting of the ballnut and the ballscrew, each angular increment (=1step) is converted into 8 μ-inches of linear translation of the manipulator leg. In summary, the robot manipulator has:

- Tracking accuracy of about 1/1000 inch,
- Maximum endpoint velocity of 3.2 inches per second,
- A 6 DOF working envelope of one cubic foot, and
- A payload capacity of about 2000 lbs.

3.2 The Passive Compliant Force/Torque Sensor

Figure 2 shows the force/torque sensor which is composed of an upper compliant platform (UCP) and a lower compliant platform (LCP) coupled together through six spring-loaded pistons arranged in a geometry similar to the mechanism of the Stewart Platform. Universal joints are used to mount the pistons to the two platforms. A gripper is attached to the LCP to perform assembly of parts. The pistons permit strain on two opposing springs acting in each piston. They are compressed or extended when resistive or gravitational forces are exerted on the gripper. Thus the force sensor mechanism also serves as a passive compliant device which provides compliance to the gripper during an assembly task. TRANS-TEK DC-DC gaging linear voltage differential transformers (LVDT) are mounted along the pistons to measure the deflection of the springs, which will be used to calculate forces/torques applied to the gripper. The supply voltage is provided by a KEPCE ATE 15-3P power supply, a very stable variable voltage power supply which is especially suitable for high precision measurement.

3.3 The Force Data Acquisition System

LVDT analog signals representing the corresponding spring deflections are processed through a CAMAC data acquisition system which consists of an Analog-to-Digital Converter (ADC) board, a Display Controller board, a Dataway display board, a CRATE controller board, and a Personal Computer (PC) interface board, all contained in a CAMAC Crate. The CAMAC Crate acts as a house for up to 25 boards and several busways for board communication, and provides DC power to the boards. The ADC board can convert up to 16 analog voltages into equivalent digital values using a sample-and-hold amplifier and a successive-approximation converter. The LVDT signals are continuously scanned and converted, and the results are then stored in the module's 16-word memory. The Dataway Display module indicates the state of all the Dataway signal lines during a Dataway cycle. It contains two 24-bit registers, designated as Data and Command register whose outputs are continuously displayed by front-panel LEDs. The Crate Controller provides an asynchronous, parallel data path between a CAMAC crate and a parallel I/O port of a computer. A 50-contact, flat-ribbon connector is used for the reception and transmission of all necessary data and control lines between the Crate Controller and the interface device which are 16 bits wide. The Crate Controller is accessed by calling assembly language routines which indicate to the system the type of information requested.

4 The Inverse Kinematic Transformation

This section presents the development of kinematic equations which can be used to convert the piston lengths measured by the LVDTs into the corresponding pose[1] of the LCP with respect to the UCP. Figure 3 shows two right-hand coordinate frames $\{\mathbf{A}\}$ and $\{\mathbf{E}\}$ assigned to the UCP and LCP, respectively. The Centroid A of the UCP is chosen to be the origin of Frame $\{\mathbf{A}\}$, the $\mathbf{z}_A$-axis is pointing outward and the $\mathbf{x}_A$-axis is perpendicular to the line connecting the two attachment points A_1 and A_6. In addition, θ_A denotes the angle between A_1 and A_2. The angles between A_1 and A_3 and between A_3 and A_5 are set to 120^o to obtain a symmetrical distribution of joints on the UCP. Similarly, the Centroid E of the LCP is the origin of Frame $\{\mathbf{E}\}$, the $\mathbf{x}_E$-axis is perpendicular to the line connecting the two attachment points E_1 and E_6, and θ_E denotes the angle between E_1 and E_2. Also the angles between E_1 and E_3 and between E_3 and E_5 are set to 120^o in order to symmetrically distribute the joints on the LCP. The Cartesian variables are chosen to be the relative pose of Frame $\{\mathbf{E}\}$ with respect to Frame $\{\mathbf{A}\}$ where the position of Frame $\{\mathbf{E}\}$ is specified by the position of its origin with respect to Frame $\{\mathbf{A}\}$. Now if we denote the angle between AA_i and $\mathbf{x}_A$ by λ_i, and the angle between EE_i and $\mathbf{x}_E$ by Λ_i for i=1,2,...,6, then

$$\Lambda_i = 60i^o - \frac{\theta_E}{2};\ \lambda_i = 60i^o - \frac{\theta_A}{2},\ \text{ for i} = 1,3,5 \tag{1}$$

and

$$\Lambda_i = \Lambda_{i-1} + \theta_E;\ \lambda_i = \lambda_{i-1} + \theta_A,\ \text{ for i} = 2,4,6. \tag{2}$$

Furthermore, if Vector ${}^E\mathbf{e}_i = (e_{ix}\ e_{iy}\ e_{iz})^T$ describes the position of the attachment point E_i with respect to Frame $\{\mathbf{E}\}$, and Vector ${}^A\mathbf{a}_i = (a_{ix}\ a_{iy}\ a_{iz})^T$ the position of the attachment point

[1] In this report, *pose* implies both *position and orientation.*

A_i with respect to Frame {**A**}, then they can be written as

$$^{E}\mathbf{e}_i = \begin{bmatrix} r_E\, cos(\lambda_i) & r_E\, sin(\lambda_i) & 0 \end{bmatrix}^T \tag{3}$$

and

$$^{A}\mathbf{a}_i = \begin{bmatrix} r_A cos(\Lambda_i) & r_A sin(\Lambda_i) & 0 \end{bmatrix}^T \tag{4}$$

for i=1,2,...,6 where r_A and r_E represent the radii of the UCP and LCP, respectively.

Let us now consider the vector diagram for an ith piston given in Figure 4. The position of Frame {**E**} is represented by Vector $^{A}\mathbf{d} = [x\ y\ z]^T$ which contains the Cartesian coordinates x, y, z of the origin of Frame {**E**} with respect to Frame {**A**}. The length vector $^{A}\mathbf{q}_i = (q_{ix}\ q_{iy}\ q_{iz})^T$, expressed with respect to Frame {**A**} can be computed by

$$^{A}\mathbf{q}_i = {}^{A}\mathbf{x}_i + {}^{A}\mathbf{e}_i \tag{5}$$

where

$$^{A}\mathbf{x}_i = {}^{A}\mathbf{d} - {}^{A}\mathbf{a}_i \tag{6}$$

$$= \begin{bmatrix} x - a_{ix} \\ y - a_{iy} \\ z - a_{iz} \end{bmatrix} = \begin{bmatrix} x - a_{ix} \\ y - a_{iy} \\ z \end{bmatrix} = \begin{bmatrix} \bar{x}_i \\ \bar{y}_i \\ \bar{z}_i \end{bmatrix} \tag{7}$$

which is a shifted vector of $^{A}\mathbf{d}$ and

$$^{A}\mathbf{e}_i = {}^{A}_{E}\mathbf{R}\ {}^{E}\mathbf{e}_i \tag{8}$$

$$= \begin{bmatrix} r_{11} & r_{12} & r_{13} \\ r_{21} & r_{22} & r_{23} \\ r_{31} & r_{32} & r_{33} \end{bmatrix} \begin{bmatrix} e_{ix} \\ e_{iy} \\ e_{iz} \end{bmatrix} = \begin{bmatrix} r_{11}e_{ix} + r_{12}e_{iy} \\ r_{21}e_{ix} + r_{22}e_{iy} \\ r_{31}e_{ix} + r_{32}e_{iy} \end{bmatrix} = \begin{bmatrix} u_i \\ v_i \\ w_i \end{bmatrix} \tag{9}$$

which is the representation of $^{A}\mathbf{e}_i$ in Frame {**A**} and $^{A}_{E}\mathbf{R}$ is the *Orientation Matrix* representing the orientation of Frame {**E**} with respect to Frame {**A**}.

Thus the length l_i of Vector $^{A}\mathbf{q}_i$ can be computed from its components as

$$l_i = \sqrt{q_{ix}^2 + q_{iy}^2 + q_{iz}^2}. \tag{10}$$

or

$$l_i = \sqrt{(\bar{x}_i + u_i)^2 + (\bar{y}_i + v_i)^2 + (\bar{z}_i + w_i)^2} \tag{11}$$

We obtain from (3)-(4)

$$e_{ix}^2 + e_{iy}^2 + e_{iz}^2 = r_E^2, \tag{12}$$

$$a_{ix}^2 + a_{iy}^2 + a_{iz}^2 = r_A^2. \tag{13}$$

and from the properties of orientation matrix

$$r_{11}^2 + r_{21}^2 + r_{31}^2 = r_{12}^2 + r_{22}^2 + r_{32}^2 = r_{13}^2 + r_{23}^2 + r_{33}^2 = 1 \tag{14}$$

and

$$\begin{aligned} r_{11}r_{12} + r_{21}r_{22} + r_{31}r_{32} &= 0 \\ r_{11}r_{13} + r_{21}r_{23} + r_{31}r_{33} &= 0 \\ r_{11}r_{13} + r_{22}r_{23} + r_{32}r_{32} &= 0. \end{aligned} \tag{15}$$

Using (12)-(15), Equation (10) can be rewritten as

$$\begin{aligned} {l_i}^2 &= x^2 + y^2 + z^2 + r_E^2 + r_A^2 + 2(r_{11}e_{ix} + r_{12}e_{iy})(x - a_{ix}) \\ &\quad +2(r_{21}e_{ix} + r_{22}e_{iy})(y - a_{iy}) + 2(r_{31}e_{ix} + r_{32}e_{iy})z \\ &\quad -2(xa_{ix} + ya_{iy}), \end{aligned} \tag{16}$$

for i=1,2,...,6.

Equation (16) represents the *closed-form* solution to the force sensor inverse kinematics in the sense that piston lengths l_i for i=1,2,...,6 which correspond to the pose of Frame $\{\mathbf{E}\}$ with respect to Frame $\{\mathbf{A}\}$ can be determined using (16).

The orientation of Frame $\{\mathbf{E}\}$ with respect to Frame $\{\mathbf{A}\}$ can be described by the orientation matrix ${}^A_E\mathbf{R}$ as shown in (9) which requires nine variables r_{ij} for i,j=1,2,3 from which six are redundant because only three are needed to specify an orientation [30]. There exist several ways to specify an orientation by three variables, but the most widely used one is the Roll-Pitch-Yaw angles α, β, and γ, which represent the orientation of Frame $\{\mathbf{E}\}$, obtained after the following sequence of rotations from Frame $\{\mathbf{A}\}$:

1. First rotate Frame $\{\mathbf{A}\}$ about the $\mathbf{x}_A$-axis an angle γ (*Yaw*),
2. Then rotate the resulting frame about the $\mathbf{y}_A$-axis an angle β (*Pitch*), and
3. Finally rotate the resulting frame about the $\mathbf{z}_A$-axis an angle α (*Roll*).

The orientation represented as above is given by (with $c\alpha \equiv \cos\alpha$, and $s\alpha \equiv \sin\alpha$)

$${}^A_E\mathbf{R} = \mathbf{R}_{RPY} = \begin{bmatrix} c\alpha\, c\beta & c\alpha\, s\beta\, s\gamma - s\alpha\, c\gamma & c\alpha\, s\beta\, c\gamma + s\alpha\, s\gamma \\ s\alpha\, c\beta & s\alpha\, s\beta\, s\gamma + c\alpha\, c\gamma & s\alpha\, s\beta\, c\gamma - c\alpha\, s\gamma \\ -s\beta & c\beta\, s\gamma & c\beta\, c\gamma \end{bmatrix}. \tag{17}$$

5 The Forward Kinematic Transformation

This section deals with the conversion of the lengths l_i for i=1,2,...,6 measured by six LVDTs into the pose of Frame $\{\mathbf{E}\}$ with respect to Frame $\{\mathbf{A}\}$. This type of conversion is the force sensor forward kinematics which can be formulated as to find a Cartesian position specified by x, y, z and an orientation specified by Roll-Pitch-Yaw angles α, β, and γ to satisfy Equation (16) for a given set of pistons lengths l_i for i=1,2,...,6. In general, there exists no closed-form solution for the above problem since Equation (16) represents a set of 6 highly nonlinear simultaneous equations with 6 unknowns. Consequently iterative numerical methods must be employed to solve the above set of nonlinear equations. In the following we will present the implementation of Newton-Raphson method for solving the forward kinematic problem.

In order to apply the Newton-Raphson method, first from (11) we define 6 scalar functions

$$f_i(\boldsymbol{\sigma}) = (\bar{x}_i + u_i)^2 + (\bar{y}_i + v_i)^2 + (\bar{z}_i + w_i)^2 - {l_i}^2 = 0 \tag{18}$$

for i=1,2,...,6, where the vector $\boldsymbol{\sigma}$ is defined as

$$\boldsymbol{\sigma} = \begin{bmatrix} \sigma_1 & \sigma_2 & \sigma_3 & \sigma_4 & \sigma_5 & \sigma_6 \end{bmatrix}^T = \begin{bmatrix} x & y & z & \alpha & \beta & \gamma \end{bmatrix}^T, \tag{19}$$

and then employ the following algorithm to solve for $\boldsymbol{\sigma}$:

Algorithm 1: Force Sensor Forward Kinematics

Step 1: Select an initial guess $\boldsymbol{\sigma}$.

Step 2: Compute the elements r_{ij} of ${}^{A}_{E}\mathbf{R}$ using (17) for i,j=1,2,3.

Step 3: Compute $\bar{x}_i$,$\bar{y}_i$, $\bar{z}_i$, using (7) and u_i, v_i, w_i using (9) for i=1,2,...,6.

Step 4: Compute $f_i(\boldsymbol{\sigma})$ and $A_{ij} = \frac{\partial f_i}{\partial \boldsymbol{\sigma}}$ using (18) for i, j=1,2,...,6.

Step 5: Compute B_i = -$f_i(\boldsymbol{\sigma})$ for i=1,2,...,6. If $\sum_{j=1}^{6} \mid B_j \mid < tolf$ (tolerance), stop and adopt $\boldsymbol{\sigma}$ as the solution.

Step 6: Solve $\sum_{j=1}^{6} A_{ij}\ \delta\sigma_j = B_i$ for $\delta\sigma_j$ for i,j=1,2,...,6 using LU decomposition. If $\sum_{j=1}^{6} \delta\sigma_j < tol\sigma$ (tolerance), stop and adopt $\boldsymbol{\sigma}$ as the solution.

Step 7: Select $\boldsymbol{\sigma}^{new} = \boldsymbol{\sigma} + \delta\boldsymbol{\sigma}$ and repeat Steps 1–7.

6 Computation of Forces/Torques

In this section, we will derive mathematical expressions which utilize the spring deflections measured by the LVDTs to compute the forces applied to the gripper. The forces will be computed with respect to Frame $\{\mathbf{A}\}$ of the UCP. When external forces are applied to the gripper, the gripper will deflect. An equilibrium is achieved when the forces created in the 6 pistons and its corresponding torques balance out the external force and torques, respectively [29]. In general, an external force applied to the gripper creates forces in the pistons and no torque about the gripper position G. An external torque which results from a pair of forces equal in magnitude, opposite in direction, and on parallel lines of action will create piston forces that cancel out each other and the resultant torque of all the torques created by the piston forces is equal to the external torque.

We proceed to consider the vector diagram in Figure 3 which represents the LCP relative to the UCP after a set of external forces and torques are applied to a point G on the gripper. The current piston lengths, $l_{i,new}$ for i=1,2,...,6 can be computed by

$$l_{i,new} = l_{i,old} + \Delta_{l_i} \tag{20}$$

where $l_{i,old}$ for i=1,2,...,6 are the piston lengths before the external forces and torques are applied and Δ_{l_i} for i=1,2,...,6 are the changes in piston lengths, measured and provided by the LVDTs. A force vector is expressed as the product of its magnitude and the unit vector of the position vector along which the force is acting [29]. The position vector ${}^{A}\mathbf{q}_i$ along which the force acts on the piston is computed by

$${}^{A}\mathbf{q}_i = {}^{A}\mathbf{d} - {}^{A}\mathbf{a}_i + {}^{A}_{E}\mathbf{R}\ {}^{E}\mathbf{e}_i \tag{21}$$

where ${}^{A}\mathbf{d}$ and ${}^{A}_{E}\mathbf{R}$ which represent the current position and orientation of Frame $\{\mathbf{E}\}$ with respect to Frame $\{\mathbf{A}\}$, respectively, are computed by applying Algorithm 1 on $l_{i,new}$. Thus the force acting on the ith piston is obtained by

$$\mathbf{F}_i = K_i\ \Delta l_i\ \frac{{}^{A}\mathbf{q}_i}{|{}^{A}\mathbf{q}_i|} \tag{22}$$

where K_i denotes the equivalent spring constant of the two springs acting in the piston and ${}^A\mathbf{q}_i/|{}^A\mathbf{q}_i|$ denotes the unit vector of the position vector along which $\mathbf{F}_i$ acts and $|{}^A\mathbf{q}_i|$ denotes the magnitude of the position vector. Furthermore, the extension, or compression, of the springs Δl_i is positive when $\mathbf{F}_i$ is tensile and negative when $\mathbf{F}_i$ is compressive. In other words, the force which the springs of the ith piston applies on the gripper is equal to -$\mathbf{F}_i$.

Thus when the gripper location G is in equilibrium, the force applied to the gripper is equal to the resultant force of the piston forces, namely

$$\mathbf{F} = \sum_{i=1}^{6} \mathbf{F}_i = \sum_{i=1}^{6} K_i \, \Delta l_i \, \frac{{}^A\mathbf{q}_i}{|{}^A\mathbf{q}_i|}. \tag{23}$$

As discussed above, from the fact that the torque about G caused by the external force applied at G is equal to zero, the external torque, M about G is equal to the resultant torque about G caused by the piston forces when the gripper is in equilibrium. Thus

$$\mathbf{M} = \sum_{i=1}^{6} {}^A\mathbf{h}_i \times \mathbf{F}_i = \sum_{i=1}^{6} {}^A\mathbf{h}_i \times K_i \, \Delta l_i \, \frac{{}^A\mathbf{q}_i}{|{}^A\mathbf{q}_i|} \tag{24}$$

where

$${}^A\mathbf{h}_i = {}^A\mathbf{d} - {}^A\mathbf{a}_i + {}^A_E\mathbf{R} \, {}^E\mathbf{g}_i, \tag{25}$$

and $\times$ denotes the vector product. The equivalent spring constant of the two springs used in the pistons is equal to 72.04 lb/inch and the minimum force the force/torque sensor can detect is about 0.2 lb.

7 Test Procedures

The FTS fingers are to be tested for grasping the cylinder interface under a relative speed of 1 inch per second with the two fingers closing simultaneously. In other words, each finger should close with a speed of 0.5 inch per second. However, the gripper currently mounted to the robot manipulator via the passive compliant mechanism is so configured that only one finger can move. In order to achieve a relative grasping speed of 1 inch/sec with 2 fingers closing simultaneously, the first finger is controlled to close with a speed of 0.5 inch per second and the payload platform (consequently the second finger) is controlled to move with a speed of 0.5 inch per second in the direction opposite to the movement of the first finger.

Before each run of the experiment, the perfect alignment between the fingers (Figure 4) and the interface (Figure 5) is established using the following procedures. First with the interface mounted rigidly to the floor as seen in Figure 6 using a vice, the payload platform pose is iteratively adjusted until no applied forces/torques are read by the force sensor. The payload pose resulting in no applied forces/torques is then recorded in the computer as the *perfect alignment pose*. Later on, before mating the fingers with the interface, from this perfect alignment pose, through proper matrix transformations, the payload platform pose can be adjusted to produce arbitrary translational and rotational misalignments or the combination of both. All misalignments are produced with respect to a coordinate frame (Figure 7) whose origin is located at the center of the two fingers and whose orientation with respect to Frame {**E**} is obtained by rotating $\mathbf{x}_E$ of Frame {**E**} an angle of 180 degrees.

8 Experimental Study Results

This section presents results of numerous experiments conducted to study the time histories of forces/torques created by mating the FTS fingers with the cylinder interface under perfect alignment and under numerous lateral and rotational misalignments.

8.1 Capture Ranges

Single-axis capture ranges of each of the selected coordinates are determined by starting from the perfect alignment, increasing the misalignment and closing the fingers at a very slow speed until it was impossible for the fingers to mate with the interface. The misalignment value immediately preceding the first time the fingers could not mate with the interface is the capture value of the coordinate under investigation. The determined capture ranges are presented in Table 1 given below.

	Lateral Misalign.	Rotational Misalign
$\mathbf{x}_I$	N/A	$\pm 6^o$
$\mathbf{y}_I$	± 0.52 in.	$\pm 6^o$
$\mathbf{z}_I$	± 0.33 in.	$\pm 8^o$

Table 1: Capture ranges of FTS fingers with cylinder interface

8.2 Graphical Representation of Test Results

In the experiments presented below, the time histories of forces/torques applied to the fingers are measured and expressed with respect to the UCP coordinate frame $\{\mathbf{A}\}$. The forces/torques are measured in two phases, the mating phase and demating stage. The LVDTs deflections are measured and recorded *on line* during the experiments, and are used to compute *off-line* the applied forces/torques using the force sensor forward kinematics and force computation equations developed in Section 5 and Section 6. The time histories of forces/torques obtained under various misalignments are processed and presented under five main groups:

- **TY Group:** This group contains graphs representing forces/torques applied under translational misalignments along the $\mathbf{Y}_I$-axis.
- **TZ Group:** This group contains graphs representing forces/torques applied under translational misalignments along the $\mathbf{Z}_I$-axis.
- **RX Group:** This group contains graphs representing forces/torques applied under rotational misalignments about the $\mathbf{X}_I$-axis.
- **RY Group:** This group contains graphs representing forces/torques applied under rotational misalignments about the $\mathbf{Y}_I$-axis.
- **RZ Group:** This group contains graphs representing forces/torques applied under rotational misalignments about the $\mathbf{Z}_I$-axis.

Each of the above five groups is divided in two subgroups, the **T Subgroup** and the **A Subgroup**, with T denoting time history graphs of forces/torques during the mating and demating of the fingers with the interface, and A for plots representing maximum forces/torques versus misalignments in a particular axis. The T Subgroup contains time history graphs for both mating and demating. However, the A Subgroup are further divided into **M Subgroup** containing graphs obtained for mating and **D Subgroup** containing graphs obtained for demating. The figure containing each individual graph is coded by two data, the amount of misalignment and the axis in which the misalignment is produced. For example, Figure **TYT-15FX** contains the time history (coded by T) of the force along the $\mathbf{x}_A$-axis (coded by FX) obtained during the mating and demating for translational misalignment of 0.15 inches (coded by 15) produced along the $\mathbf{y}_I$-axis (coded by TY). Figure **RZAM-TY** contains the plot (coded by A) of maximum torque about the $\mathbf{y}_A$-axis (coded by TY) versus rotational misalignments produced about the $\mathbf{z}_I$-axis (coded by RZ) during the mating (coded by M). The contents of the obtained graphs are summarized as follows:

1. **Translational Misalignments along the $\mathbf{Y}_I$-Axis, Group TY**

   - Figures TYT-00FX, -FY, -FZ, -FG, -TX, -TY, and -TZ show the time histories of forces/torques applied along/about the $\mathbf{x}_A$-axis, $\mathbf{y}_A$-axis, $\mathbf{z}_A$-axis, and the gripper $\mathbf{G}_I$-axis, respectively for mating and demating the FTS finger with the interface under perfect alignment. The mating occurs at about 0.4 second and the demating at about 1.4 second. All graphs have similar force/torque responses in the sense that applied forces/torques are zero before the mating, are disturbed during the mating (first transition), settle down to a steady-state constant value after the fingers are completely mated with the interface (second transition), are disturbed again during the demating (third transition), and finally settle down to zero value after the demating is completed (fourth transition).
   - Figures TYT-05FX, -FY, -FZ, -FG, -TX, -TY, and -TZ show the time histories of forces/torques applied along/about the $\mathbf{x}_A$-axis, $\mathbf{y}_A$-axis, $\mathbf{z}_A$-axis, and the gripper $\mathbf{G}_I$-axis, respectively for mating and demating the FTS finger with the interface under a translational misalignment of 0.05 inches along the $\mathbf{Y}_I$-axis. The mating occurs at about 0.2 second and the demating at about 1.4 second.
   - Figures TYT-10FX, -FY, -FZ, -FG, -TX, -TY, and -TZ show the time histories of forces/torques applied along/about the $\mathbf{x}_A$-axis, $\mathbf{y}_A$-axis, $\mathbf{z}_A$-axis, and the gripper $\mathbf{G}_I$-axis, respectively for mating and demating the FTS finger with the interface under a translational misalignment of 0.10 inches along the $\mathbf{Y}_I$-axis. The mating occurs at about 0.4 second and the demating at about 1.4 second.
   - Figures TYT-15FX, -FY, -FZ, -FG, -TX, -TY, and -TZ show the time histories of forces/torques applied along/about the $\mathbf{x}_A$-axis, $\mathbf{y}_A$-axis, $\mathbf{z}_A$-axis, and the gripper $\mathbf{G}_I$-axis, respectively for mating and demating the FTS finger with the interface under a translational misalignment of 0.15 inches along the $\mathbf{Y}_I$-axis. The mating occurs at about 0.3 second and the demating at about 1.5 second.
   - Figures TYT-20FX, -FY, -FZ, -FG, -TX, -TY, and -TZ show the time histories of forces/torques applied along/about the $\mathbf{x}_A$-axis, $\mathbf{y}_A$-axis, $\mathbf{z}_A$-axis, and the gripper $\mathbf{G}_I$-axis, respectively for mating and demating the FTS finger with the interface under

a translational misalignment of 0.20 inches along the $\mathbf{Y}_I$-axis. The mating occurs at about 0.4 second and the demating at about 1.4 second.

- Figures TYT-25FX, -FY, -FZ, -FG, -TX, -TY, and -TZ show the time histories of forces/torques applied along/about the $\mathbf{x}_A$-axis, $\mathbf{y}_A$-axis, $\mathbf{z}_A$-axis, and the gripper $\mathbf{G}_I$-axis, respectively for mating and demating the FTS finger with the interface under a translational misalignment of 0.25 inches along the $\mathbf{Y}_I$-axis. The mating occurs at about 0.4 second and the demating at about 1.3 second.
- Figures TYT-30FX, -FY, -FZ, -FG, -TX, -TY, and -TZ show the time histories of forces/torques applied along/about the $\mathbf{x}_A$-axis, $\mathbf{y}_A$-axis, $\mathbf{z}_A$-axis, and the gripper $\mathbf{G}_I$-axis, respectively for mating and demating the FTS finger with the interface under a translational misalignment of 0.30 inches along the $\mathbf{Y}_I$-axis. The mating occurs at about 0.4 second and the demating at about 1.6 second.
- Figures TYT-35FX, -FY, -FZ, -FG, -TX, -TY, and -TZ show the time histories of forces/torques applied along/about the $\mathbf{x}_A$-axis, $\mathbf{y}_A$-axis, $\mathbf{z}_A$-axis, and the gripper $\mathbf{G}_I$-axis, respectively for mating and demating the FTS finger with the interface under a translational misalignment of 0.35 inches along the $\mathbf{Y}_I$-axis. The mating occurs at about 0.4 second and the demating at about 1.7 second.
- Figures TYT-40FX, -FY, -FZ, -FG, -TX, -TY, and -TZ show the time histories of forces/torques applied along/about the $\mathbf{x}_A$-axis, $\mathbf{y}_A$-axis, $\mathbf{z}_A$-axis, and the gripper $\mathbf{G}_I$-axis, respectively for mating and demating the FTS finger with the interface under a translational misalignment of 0.40 inches along the $\mathbf{Y}_I$-axis. The mating occurs at about 0.4 second and the demating at about 1.5 second.
- Figures TYT-45FX, -FY, -FZ, -FG, -TX, -TY, and -TZ show the time histories of forces/torques applied along/about the $\mathbf{x}_A$-axis, $\mathbf{y}_A$-axis, $\mathbf{z}_A$-axis, and the gripper $\mathbf{G}_I$-axis, respectively for mating and demating the FTS finger with the interface under a translational misalignment of 0.45 inches along the $\mathbf{Y}_I$-axis. The mating occurs at about 0.3 second and the demating at about 1.4 second.
- Figures TYAM-FX, -FY, -FZ, -FG, -TX, -TY, and -TZ show the relationship between the translational misalignments produced along the $\mathbf{y}_I$-axis and the maximum forces/torques applied along/about the $\mathbf{x}_A$-axis, $\mathbf{y}_A$-axis, $\mathbf{z}_A$-axis, and the gripper $\mathbf{G}_I$-axis, respectively during the mating process.
- Figures TYAD-FX, -FY, -FZ, -FG, -TX, -TY, and -TZ show the relationship between the translational misalignments produced along the $\mathbf{y}_I$-axis and the maximum forces/torques applied along/about the $\mathbf{x}_A$-axis, $\mathbf{y}_A$-axis, $\mathbf{z}_A$-axis, and the gripper $\mathbf{G}_I$-axis, respectively during the demating process.

2. **Translational Misalignments along the $\mathbf{Z}_I$-Axis, Group TZ:** Similar to above case.
3. **Rotational Misalignments about the $\mathbf{X}_I$-Axis, Group RX:** Similar to above case.
4. **Rotational Misalignments about the $\mathbf{Y}_I$-Axis, Group RY:** Similar to above case.
5. **Rotational Misalignments about the $\mathbf{Z}_I$-Axis, Group RZ:** Similar to above case.

9 Conclusions and Recommendations

This report has presented an experimental study of the performance of a pair of the FTS fingers in mating with a cylinder interface. First it presented the objectives of the study and then described the testbed to be used in the study. It then presented a closed-form solution for the force inverse kinematics and a numerical solution using Newton-Raphson Method for the force forward kinematics. Mathematical expressions were derived to compute forces/torques applied to the finger. After that, the report presented the results of numerous experiments conducted to study the characteristics and feasibility of the fingers in mating and demating with the interface. Single-axis capture ranges for the interface were empirically determined. Applied forces during the mating and demating of the fingers with the interface were measured under various rotational and translational misalignments, and then graphically presented. Plots of applied forces versus misalignments showed that the forces were generally proportional to the misalignments except for some few cases in which the misalignment caused the fingers to hit different mating surfaces resulting in unexplainable force/torque transitions.

Based on the results of our study, we recommend the following:

- The testing process is very time-consuming. On the average, each experiment which obtained data for computing applied forces/torques along/about the $\mathbf{x}_A$, $\mathbf{y}_A$, $\mathbf{z}_A$ and along the gripper axis, took about 30 minutes to prepare and run, and a total of 25 experiments were performed. We recommend that computer software and hardware be developed to automate the complete testing process.

- Because of the time-consuming nature of the testing process, only mating and demating under single-axis misalignments were considered. In order to make the testing results more useful and realistic to the re-design and improvement of the FTS fingers and interface, combinational misalignments in multiple axes should be considered in future testing.

In conclusion, in order to achieve an operational set of fingers and interfaces, an iterative and cooperative development process should be adopted. The design and fabricator of the FTS fingers should use obtained test data to improve the design of the fingers and interfaces and independent laboratory should test and re-evaluate the interfaces and the fingers based on the mating/demating performance. This process should be repeated until a satisfactory level of performance is achieved.

References

[1] Catalano, D.A., "WP-04 Orbit Replaceable Unit Robotics Maintenance Final Test Report," *Analex Corp.*, GSFC, November 1990

[2] Stewart, D., "A Platform with Six Degrees of Freedom," *Proc. Institute of Mechanical Engineering*, Vol. 180, Part 1, No. 5, pp. 371-386, 1965-1966.

[3] Dieudonne, J.E. et al, "An Actuator Extension Transformation for a Motion Simulator and an Inverse Transformation Applying Newton-Raphson's Method," *NASA Technical Report D-7067*, 1972.

[4] Hoffman, R., and McKinnon, M.C., "Vibration Modes of an Aircraft Simulator Motion System," *Proc. The Fifth World Congress for the Theory of Machines and Mechanisms, an ASME Publication*, pp. 603-606, 1979.

[5] McCallion, H., and Truong, P.D., "The Analysis of a Six-Degree-of-Freedom Work Station for Mechanised Assembly," *Proc. The Fifth World Congress for the Theory of Machines and Mechanisms, an ASME Publication*, pp. 611-616, 1979.

[6] Hunt, K. H., *Kinematic Geometry of Mechanisms*, Oxford University, London 1978.

[7] Sugimoto, K. and Duffy, J., "Application of Linear Algebra to Screw Systems," *Mech. Mach. Theory*, Vol. 17, No. 1, pp. 73-83, 1982.

[8] Hunt, K. H., "Structural Kinematics of in-parallel-actuated Robot Arms," *Trans. ASME, J. Mech., Transmis., Automa. in Des.*, Vol. 105, pp. 705-712, 1983.

[9] Premack, Timothy et al, "Design and Implementation of a Compliant Robot with Force Feedback and Strategy Planning Software," *NASA Technical Memorandum 86111*, 1984.

[10] Nguyen, C.C., Pooran, F.J., and Premack, T., "Control of Robot Manipulator Compliance," in *Recent Trends in Robotics: Modeling, Control and Education*, edited by M. Jamshidi, J.Y.S. Luh, and M. Shahinpoor, North Holland, New York, pp. 237-242, 1986.

[11] Yang, D. C. and Lee, T. W., "Feasibility Study of a Platform Type of Robotic Manipulators from a Kinematic Viewpoint," *Trans. ASME Journal of Mechanisms, Transmissions, and Automation in Design*, Vol. 106. pp. 191-198, June 1984.

[12] Mohammed, M. G. and Duffy, J., "A Direct Determination of the Instantaneous Kinematics of Fully Parallel Robotic Manipulators," *ASME Journal of Mechanisms, Transmissions, and Automation in Design*, Vol. 107 pp. 226-229, 1985.

[13] Fichter, E.F., "A Stewart Platform-Based Manipulator: General Theory and Practical Construction," *Int. Journal of Robotics Research*, pp. 157-182, Summer 1986

[14] Sugimoto, K., "Kinematic and Dynamic Analysis of Parallel Manipulators by Means of Motor Algebra," *ASME Journal of Mechanisms, Transmissions, and Automation in Design*, pp. 1-5, Dec. 1986.

[15] Lee, K. M., Chao, A., and Shah, D. K., "A Three Degrees of Freedom In-parallel Actuated Manipulator," *Proc. IASTED Int. Conf.*, pp. 134-138, 1986.

[16] Rees-Jones, J., "Cross Coordinate Control of Robotic Manipulators," in *Proceedings of the International Workshop on Nuclear Robotic Technologies and Applications, Present and Future*, University of Lancaster, UK, June 29-July 1, 1987.

[17] Behi, F., "Kinematic Analysis for a Six-Degree-of-Freedom 3-PRPS Parallel Mechanism," *IEEE Journal of Robotics and Automation*, Vol. 5, No. 5, pp. 561-565, October 1988.

[18] Sharon, A., Hogan, N., Hardt, D., "High-Bandwidth Force Regulation and Inertia Reduction Using a Macro/Micro Manipulator System," *Proc. IEEE International Conference on Robotics and Automation*, pp. 261-266, Philadelphia, PA, April 1988.

[19] Sugimoto, K., "Computational Scheme for Dynamic Analysis of Parallel Manipulators," in *Trends and Developments in Mechanisms, Machines, and Robotics-1988, ASME Proceedings of the 20th Biennial Mechanisms Conference*, 1988.

[20] Kerr, D. R., "Analysis, Properties, and Design of a Stewart-Platform Transducer,"in *Trends and Developments in Mechanisms, Machines, and Robotics-1988, ASME Proceedings of the 20th Biennial Mechanisms Conference*, 1988.

[21] Nguyen, C.C., Pooran, F.J., "Adaptive Force/Position Control of Robot Manipulators with Closed-Kinematic Chain Mechanism," in *Robotics and Manufacturing: Recent Trends in Research, Education, and Application*, edited by M. Jamshidi et al, ASME Press, New York, pp. 177-186, 1988.

[22] Griffis, M., Duffy, J., "A Forward Displacement Analysis of a Class of Stewart Platforms," *Journal of Robotic Systems*, Vol. 6, pp. 703-720, 1989.

[23] Nguyen, C.C., and Pooran, F.J., "Kinematic Analysis and Workspace Determination of A 6 DOF CKCM Robot End-Effector," *Journal of Mechanical Working Technology*, Vol. 20, pp. 283-294, 1989.

[24] Nguyen, C.C., and Pooran, F.J., "Dynamical Analysis of 6 DOF CKCM Robot End-Effector for Dual-Arm Telerobot Systems," *Journal of Robotics and Autonomous Systems*, Vol. 5, pp. 377-394, 1989.

[25] Nanua, P., Waldron, K.J., Murthy, V., "Direct Kinematic Solution of a Stewart Platform," *IEEE Trans. Robotics and Automation*, Vol. 6, No. 4, pp. 438-444, 1990.

[26] Nguyen, C.C., and Pooran, F.J., "Learning-Based Control of a Closed-Kinematic Chain Robot End-Effector Performing Repetitive Tasks," *International Journal of Microcomputer Applications*, Vol. 9, No. 1, pp. 9-15, 1990.

[27] Nguyen, C.C., Antrazi, S., Zhou, Z-L, "Trajectory Planning and Kinematic Control of a Stewart Platform-Based Manipulator," *Proc. 5th International Conference on CAD/CAM Robotics and Factories of the Future*, Norfolk, Virginia, December 1990.

[28] Nguyen, C.C., Antrazi, S., Zhou, Z-L, Campbell, Jr., C.E., "Experimental Study of Motion Control and Trajectory Planning for a Stewart Platform Robot Manipulator," *Proc. IEEE International Conference on Robotics and Automation*, Sacramento, California, April 1991.

[29] Goodman, L.E. and Warner, W.H., "Statics," *Wadsworth Publishing Company, Inc.,*, Belmont, California, 1963.

[30] Fu, K.S. et.al., *Robotics: Control, Sensing, Vision, and Intelligence* , McGraw-Hill, New York, 1987.

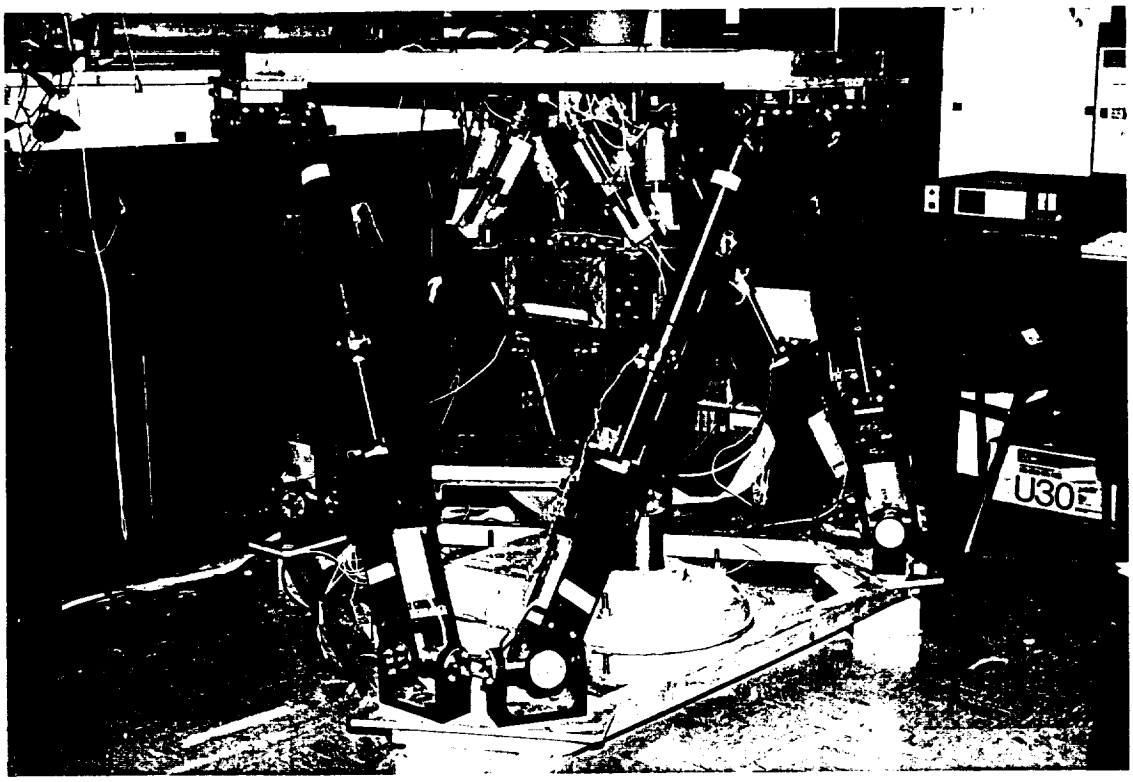

Figure 1: The 6 DOF robot manipulator serving as the study testbed

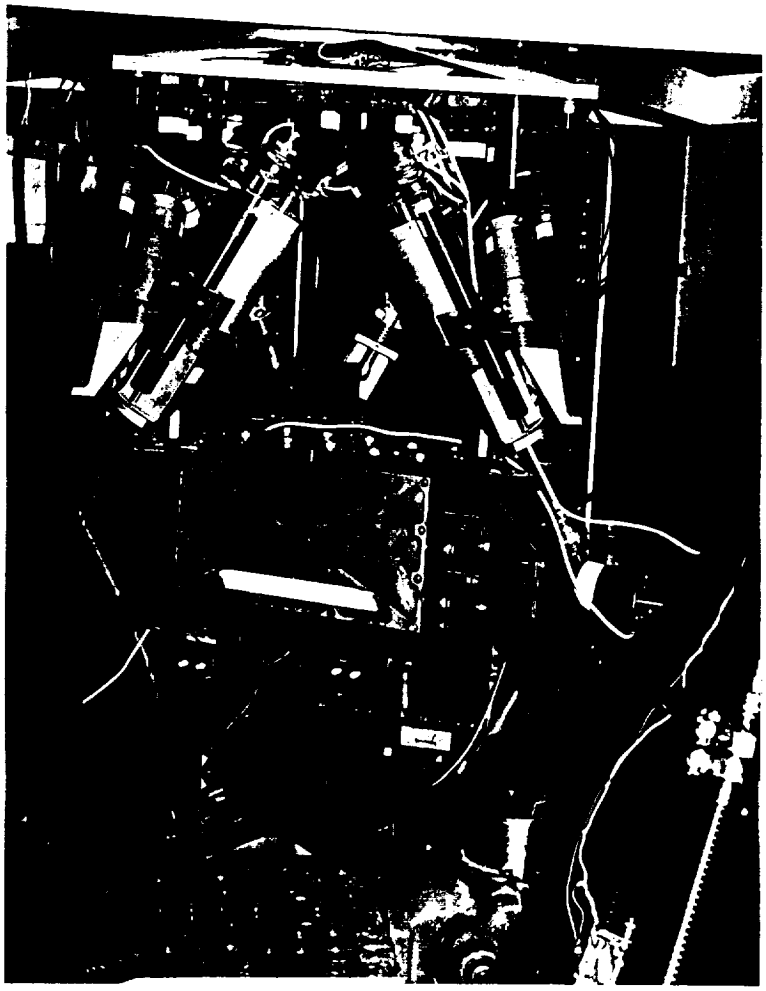

Figure 2: The passive compliant force/torque sensor

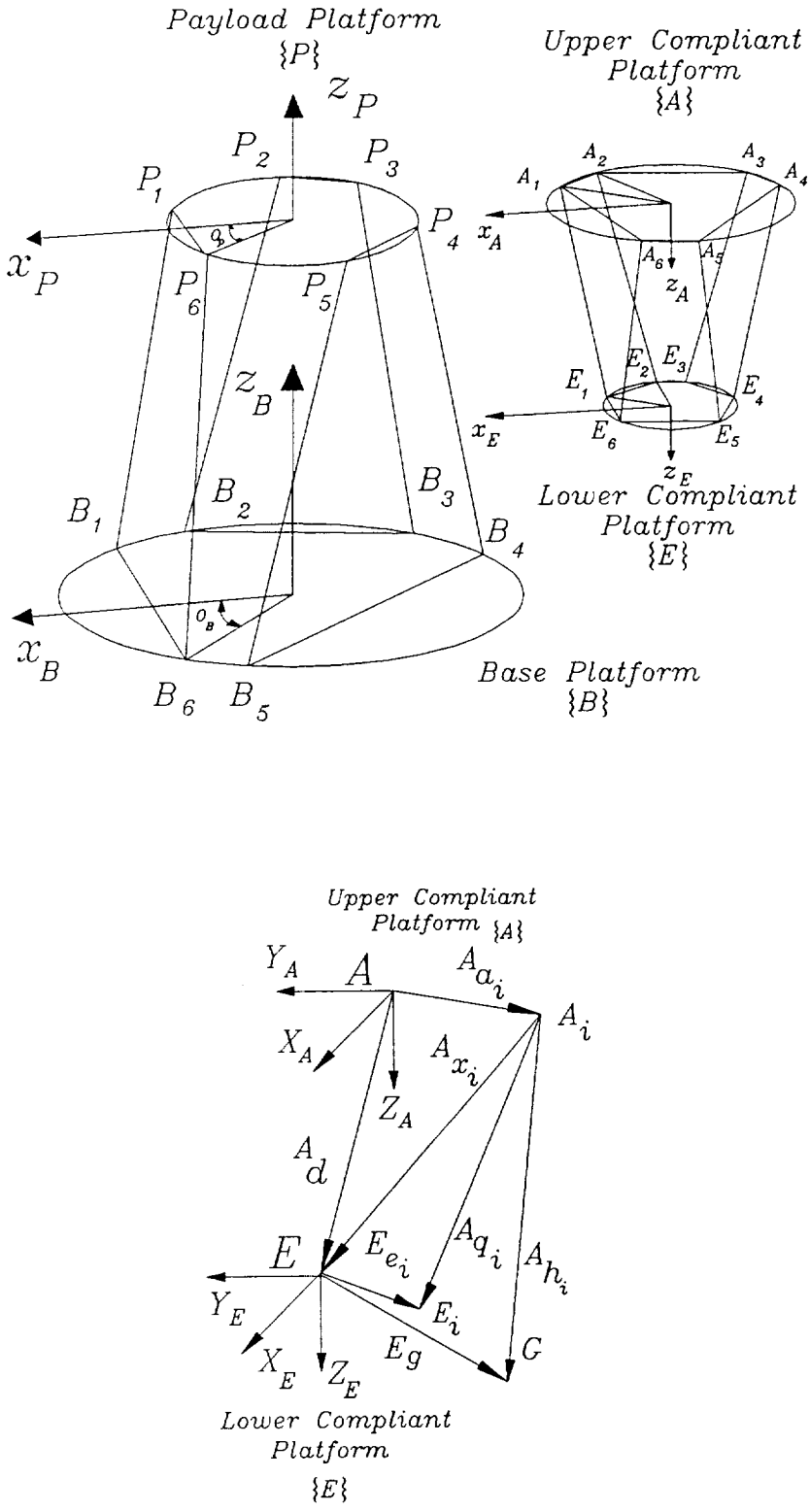

Figure 3: Coordinate frame assignment and vector diagram

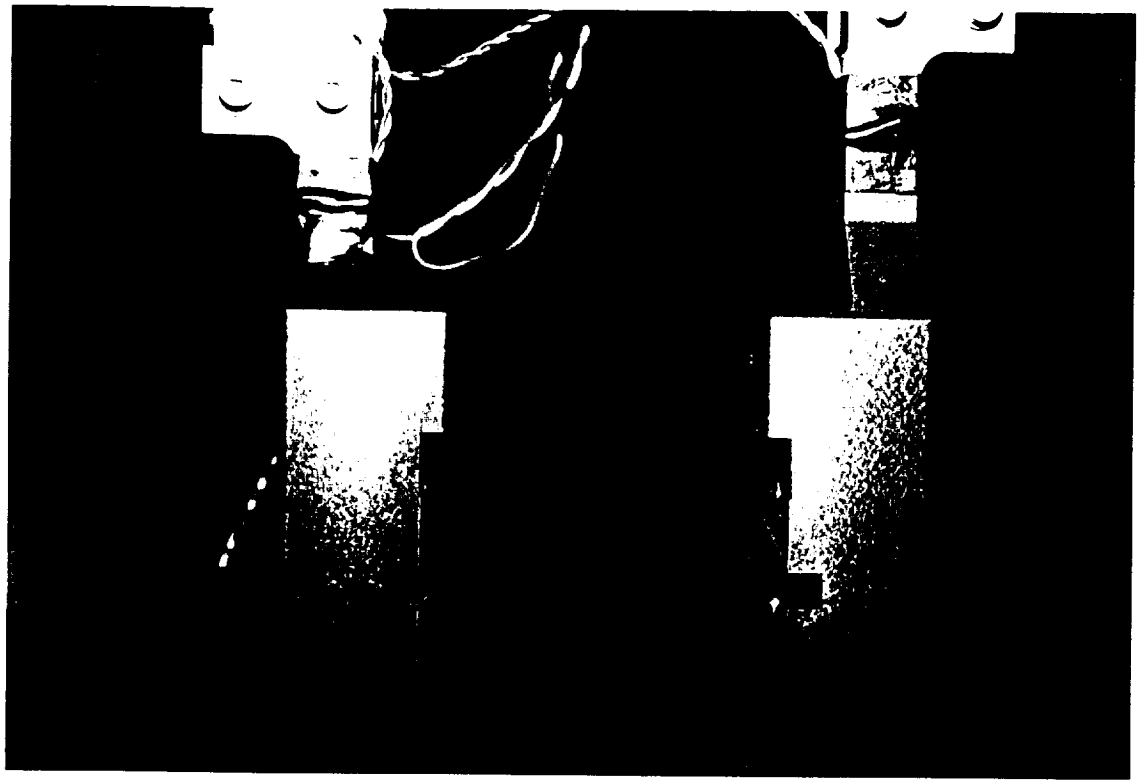

Figure 4: The Flight Telerobot Servicer (FTS) fingers

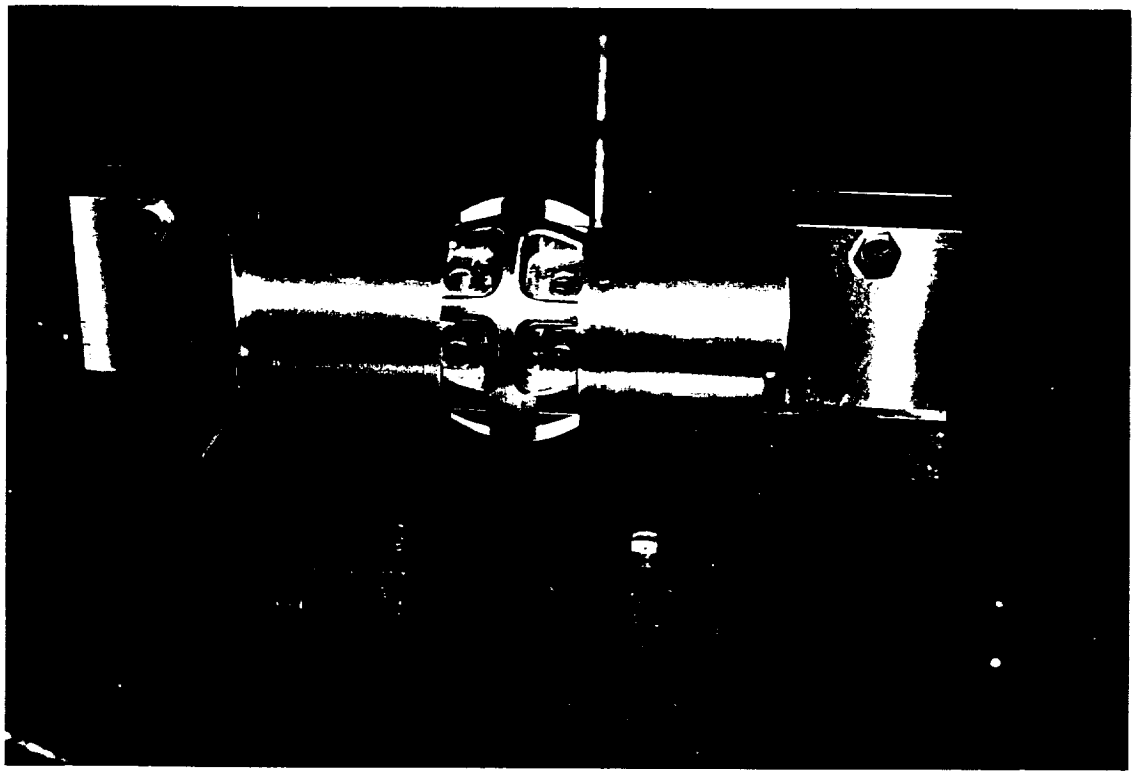

Figure 5: The cylinder interface

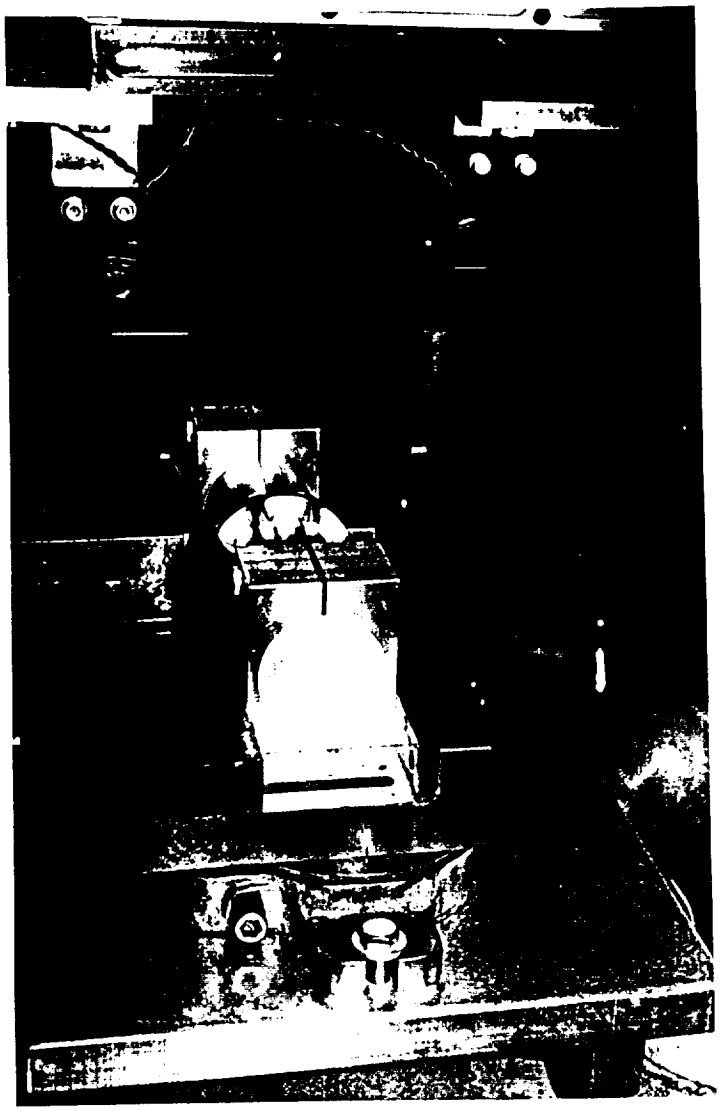

Figure 6: The test setup

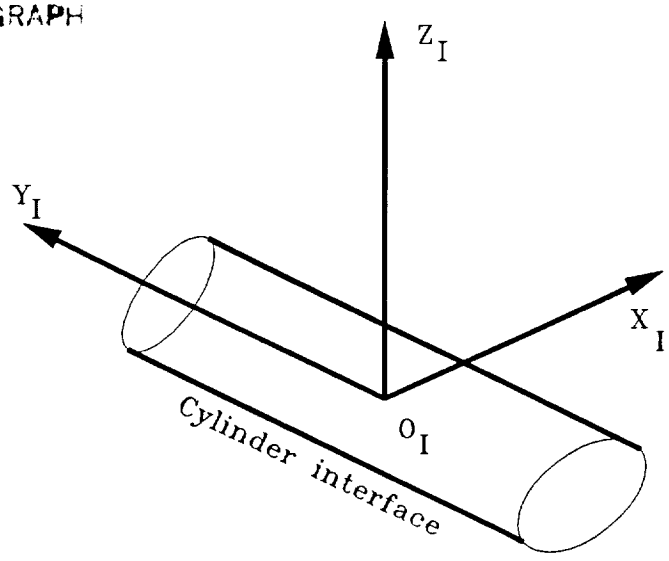

Figure 7: Misalignment coordinate frame assigned to the interface